GEOPHYSICS, VOL. 77, NO. 4 (JULY-AUGUST 2012); P. B177–B185, 10 FIGS., 1 TABLE.
10.1190/GEO2011-0401.1

Case History

Common-reflection-surface imaging of shallow and ultrashallow reflectors

Gian Piero Deidda[1], Enzo Battaglia[1], and Zeno Heilmann[2]

ABSTRACT

We analyzed the feasibility of the common-reflection-surface (CRS) stack for near-surface surveys as an alternative to the conventional common midpoint (CMP) stacking procedure. The data-driven, less user-interactive CRS method could be more cost efficient for shallow surveys, where the high sensitivity to velocity analysis makes data processing a critical step. We compared the results for two field data sets collected to image shallow and ultrashallow reflectors: an example of shallow P-wave reflection for targets in the first few hundred meters, and an example of SH-wave reflection for targets in the first 10 m. By processing the shallow P-wave records using the CMP method, we imaged several nearly horizontal reflectors with onsets from 60 to about 250 ms. The CRS stack produced a stacked section more suited for a subsurface interpretation, without any preliminary formal and time-consuming velocity analysis, because the imaged reflectors possessed greater coherency and lateral continuity. With CMP processing of the SH-wave records, we imaged a dipping bedrock interface below four horizontal reflectors in unconsolidated, very low velocity sediments. The vertical and lateral resolution was very high, despite the very shallow depth: the image showed the pinchout of two layers at less than 10 m depth. The numerous traces used by the CRS stack improved the continuity of the shallowest reflector, but the deepest overburden reflectors appear unresolved, with not well-imaged pinchouts. Using the kinematic wavefield attributes determined for each stacking operation, we retrieved velocity fields fitting the stacking velocities we had estimated in the CMP processing. The use of CRS stack could be a significant step ahead to increase the acceptance of the seismic reflection method as a routine investigation method in shallow and ultrashallow seismics.

INTRODUCTION

The shallow seismic reflection method is a well-established tool suitable for imaging near-surface structure from a few meters to a few hundred meters depth. Both P- and S-wave (and usually SH-wave) reflection methods have proven useful in many engineering, geotechnical, environmental, and hydrogeological studies (e.g., Goforth and Hayward, 1992; Woorely et al., 1993; Ghose et al., 1998; Liberty, 1998; Benjumea et al., 2003; Guy et al., 2003; Bradford et al., 2006; Pugin et al., 2009). To date, however, engineers, geotechnicians, and hydrogeologists still do not consider them as routine investigation methods, preferring other geophysical methods, such as seismic refraction and surface wave methods or electrical resistivity and electromagnetic methods. The costs of data acquisition and data processing have discouraged the extensive use of seismic reflection methods in the above-mentioned fields. The high costs of seismic reflection data acquisition has been widely reduced by instrumentation and methodology developments during the last 15 years. Van der Veen and Green (1998) and Van der Veen et al. (2001) using a landstreamer of gimballed geophones showed that P-wave data of quality similar to data acquired with spiked geophones can be collected at higher rates with fewer field personnel. Pugin et al. (2009) described a Minivib/landstreamer acquisition system with which they routinely acquire P- or S-wave data from

Manuscript received by the Editor 8 October 2011; revised manuscript received 14 February 2012; published online 14 June 2012.
[1]University of Cagliari, Department of Civil and Environmental Engineering and Architecture, Cagliari, Italy. E-mail: gpdeidda@unica.it; ebattaglia@unica.it.
[2]CRS4, Imaging and Numerical Geophysics, Pula, Italy. E-mail: zeno@crs4.it.

around 1000 shotpoint/day, gaining production rates from two to 10 times the rate usually expected using planted geophones. Sambuelli et al. (2001) described a special horizontal receiver that detects horizontal movements better than standard horizontal geophones. It allows collection of SH-wave records with minimal P-wave contamination performing single shots and avoiding the extra processing (amplitude adjustments, removal of time-break variations, and trace-to-trace subtraction) usually requested when two shots are used by striking the source in opposite directions. So, landstreamers, vibrating sources, and newly designed geophones have greatly reduced costs for data acquisition.

Costs for data processing, however, could still be reduced, as it often requires a large time commitment. Unfortunately, the success of shallow seismic reflection surveys greatly depends on the processing, and in particular on the detail with which velocity analysis and residual static corrections are carried out. In the near surface, seismic velocities have large and sometimes unexpected variations; e.g., they may change by an order of magnitude within only a few meters in vertical and/or horizontal directions. Such pronounced velocity variations, uncommon at the typical depths of conventional seismic reflection surveys, cause complex reflection traveltime distortions and consequently elaborate velocity analysis. In such cases, prestack depth migration (PSDM) is a procedure providing more accurate and more detailed shallow seismic images in comparison with the conventional common midpoint (CMP) stacking methods based on normal moveout (NMO)/dip moveout (DMO) stack (Pasasa et al., 1998; Bradford and Sawyer, 2002; Bradford et al., 2006; Bruno et al., 2010). Whatever the processing procedure used, however, stacking velocities must always be determined with extraordinary emphasis to obtain good stacked sections, correctly interpretable from both the structural and the stratigraphic points of view. CMP-by-CMP velocity analysis with the requested accuracy is time-consuming and usually the most expensive processing step for shallow seismic imaging. Moreover, since traditional NMO-correction techniques in the processing of seismic data can produce stretch-related artifacts, severe stretch muting is usually required even if at the expense of the signal-to-noise ratio (S/N). For shallow and ultrashallow seismic reflection data, all these aspects involve high processing costs due to poorly automated, and as such, time-consuming processing steps.

In this paper we analyze and discuss a possible solution to these processing-related problems, namely, to substitute for processing of shallow and ultrashallow seismic reflection data the conventional or standard CMP stacking method with the common-reflection-surface (CRS) stack method (e.g., Mann et al., 1999; Jäger et al., 2001). During the last decade, the CRS stack established itself as a promising new approach for time domain imaging and velocity analysis in oil and gas exploration. It is based on a generalized velocity analysis and stacking procedure that employs multiparameter stacking surfaces to obtain a simulated zero-offset section in a data-driven way. Unlike CMP-based methods, the stacking process is not confined only to single CMP gathers (offset direction), but it also includes neighboring CMPs (midpoint direction) to form so-called CRS supergathers. Such a supergather covers all traces that contain energy reflected from a certain common-reflector-segment in depth centered at the theoretical reflection point of the zero-offset ray. Different from the NMO/DMO method, which assumes a planar dipping reflector segment, the CRS method assumes a reflector-segment of arbitrary dip and curvature including diffraction points and planar reflectors (Hertweck et al., 2007). The spatial stacking operator allows a more stable velocity analysis, better stacking results for targets such as flat-layered or steeply dipping reflectors as well as diffractors or faults, and/or the use of sparser surveys without loss in imaging quality (Gierse et al., 2009). Due to the data-driven implementation of the multiparameter velocity analysis, time-consuming human interaction in prestack velocity analysis can be avoided, making the whole imaging process less user-interactive and more cost efficient. However, if velocity information is needed for other tasks such as poststack and/or prestack time or depth migration, time-to-depth conversion and/or geotechnical site characterization, it can be obtained from the kinematic wavefield attributes that are determined for each stacking operation through coherence (semblance) analysis on the prestack data. This process fully replaces the traditional CMP velocity analysis (e.g., Perroud and Tygel, 2005) and allows the replacement of the 1D Dix velocity conversion (Dix, 1955) with a 2D tomographic inversion approach (Duveneck, 2004).

To investigate the capability of the CRS method to image near-surface structures, we compared the results obtained from processing two different field data sets with CMP and CRS procedures. The first of them consists of P-wave data collected in a framework of shallow seismic reflection surveys carried out to improve understanding of a hydrogeologic structure. The second data set, instead, consists of SH-wave data collected to image multiple reflectors less than 10 m deep in a geotechnical characterization. In both cases the CRS stack, working in a fully automatic way, quickly gave stacked sections of high quality without the need for any preliminary time-consuming velocity analysis. To date, many successful examples of 2D and 3D CRS applications document its imaging capabilities both in simple and complex areas (e.g., Mann et al., 1999; Bergler et al., 2002; Heilmann et al., 2006; Pruessmann et al., 2008), but we are unaware of any examples reporting shallow and ultrashallow CRS cases. Our results, therefore, further document the capabilities of the CRS stack in the specific field of shallow seismic reflection surveys. We believe that the use of CRS stacking, in turn, can increase acceptance of shallow seismic reflection as a routine investigation method by engineers, geotechnicians, and hydrogeologists.

A BRIEF INTRODUCTION OF CRS STACK

With the aim of making the following sections more easily readable, we briefly introduce here some background information about the CRS stack, recalling its basic principle and the meaning of the most important parameters we used to process our field data sets. For a more exhaustive and specific explanation of the CRS stack other sources in literature are available (e.g., Gelchinsky et al., 1999a, 1999b; Jäger et al., 2001; Zhang et al., 2001; Höcht, 2002; Mann, 2002; Bergler, 2004; Hertweck et al., 2007; Baykulov et al., 2011).

The CRS stack can be understood as a generalization of the classical CMP stack. The latter is based on assuming a macrovelocity model made of homogeneous layers separated by horizontal interfaces. The CMP stack operator is usually defined by a hyperbolic traveltime approximation in the offset direction

$$t_{hyp}^2(h) = t_0^2 + \frac{4h^2}{V_{\mathrm{NMO}}^2}, \qquad (1)$$

where h is the half-offset coordinate and t_0 is the zero-offset traveltime. The well-known NMO velocity, V_{NMO}, is the only parameter

that needs to be known to sum up all signals reflected at a common reflection point in depth. However, for a dipping reflector, the so-called reflection point smearing occurs because the midpoint is no longer a vertical projection of the depth point to the surface. The CRS stack method solves this limitation by adding a midpoint coordinate to the traveltime approximation 1 at the cost of introducing two additional stacking parameters. As a consequence, this spatial stacking operator sums up all amplitudes originating from a CRS. The hyperbolic CRS stack operator is defined by the following approximation

$$t_{hyp}^2(x_m, h) = \left[t_0 + \frac{2 \cdot \sin\alpha}{v_0}(x_m - x_0)\right]^2 + \frac{2 \cdot t_0 \cdot \cos^2\alpha}{v_0} \cdot \left[\frac{(x_m - x_0)^2}{R_N} + \frac{h^2}{R_{NIP}}\right], \quad (2)$$

where x_m and h are the midpoint and half-offset coordinates, respectively. The summation result is placed in the zero-offset section at the point (x_0, t_0), which represents traveltime and emergence point of the zero-offset (central) ray, i.e., the ray reflected at the center of the common reflection segment. The three stacking parameters in function 2, α, R_{NIP}, and R_N, are the emergence angle of the zero-offset ray and the two wavefront curvatures of the theoretical eigenwaves denoted as normal incident point wave and normal wave (Hubral, 1983; Jäger et al., 2001). These kinematic wavefield attributes are determined automatically from the prestack data by means of coherence analysis. Finally, v_0 denotes the near-surface velocity in x_0. This a priori information is needed because v_0 relates the searched-for reflection traveltime surface to the physically interpretable stacking parameters α, R_{NIP}, and R_N.

For stacking along the spatial CRS operator, a spatial definition of the stacking aperture is required. In practice, the choice of the right stacking apertures is crucial as it substantially affects seismic resolution and S/N. The software used to process the shallow and ultrashallow seismic data in the following examples is the CRS stack implementation, version 4.7, described in Mann (2002) and developed at the University of Karlsruhe. This implementation employs a tapered traveltime-dependent stacking aperture of elliptic shape in the midpoint/offset plane with user-defined half-axes given by a midpoint aperture for $h = 0$ and an offset aperture for $x_m = x_0$. This choice accounts for the approximate nature of the CRS operator, which is basically a second-order Taylor expansion of the reflection traveltime centered at h=0, $x_m = x_0$. By default, the software creates two stacked sections; one that corresponds to the user-defined apertures, and one that corresponds to a midpoint aperture that is an approximation of the Fresnel zone calculated from the stacking parameters and the estimated peak-frequency of the source wavelet (e.g., Mann, 2002).

FIELD EXAMPLE 1 — SHALLOW P-WAVE DATA SET

Standard CMP processing

The data described in this example were collected during a seismic reflection survey conducted to delineate and characterize a multilayer confined aquifer and its confining units in a paleolake environment near Cagliari (Sardinia, Italy). P-wave data were acquired along a line 630 m long using a standard CMP roll-along technique in an end-on configuration with 24 active 50-Hz vertical receivers and a near offset of 25 m. A 0.15 kg explosive source was buried at approximately 2 m depth for each shot position. Both geophone and source spacing of 5 m provided twelvefold CMP coverage with a CMP spacing of 2.5 m. An analog 50 Hz low-cut filter was used to attenuate the ground roll, which was recorded as having very high amplitudes at this site in a preliminary walkaway noise test. Three representative field records are shown in Figure 1.

In addition to the typical ground roll, several clear reflections can be observed in each record. The spectral content of the recorded data ranges from about 20 to 300 Hz at near offsets, and up to 180 Hz at far offsets. Peak amplitudes fall between 20–40 Hz and belong to ground roll, while the dominant frequency of the reflected signals is around 70–80 Hz on average. The data processing steps outlined in Table 1 were performed on a laptop using Parallel Geoscience Corp.'s SPW seismic package. To attenuate low-frequency ground roll components still evident in the records and high-frequency noises, Butterworth filtering (50–250 Hz, 24 dB/octave) was used; *f-k* muting helped us to filter out ground roll with higher frequencies (up to about 60 Hz), some of which had a small amount of spatial aliasing, but also to filter out the aliased portions of other linear noises (e.g., critically refracted wave and airwave), sometimes evident in the records. Figure 2 shows the filtered records shown in Figure 1. Removal of time-break variations

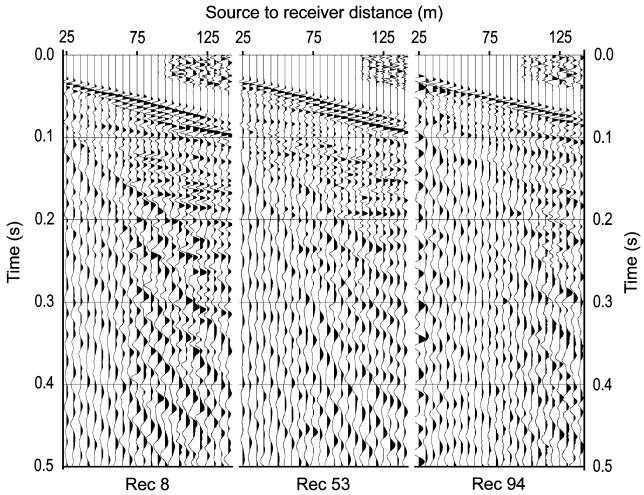

Figure 1. Raw shot gathers from three locations along the line. For display purposes, AGC scaling with a 100-ms window has been applied.

Table 1. Data processing steps.

Preprocessing	Field geometry
	Trace and record editing
	Band-pass filtering
	f-k muting
Main processing	Velocity analysis
	NMO correction (30% stretch mute)
	Residual statics
	CMP stack

due to unavoidable little differences among source depths completed the preprocessing. Since the topography at this site is flat, no field statics were applied.

Particular attention to velocity analysis and to residual static corrections was needed to obtain high-amplitude stacked traces. As shown by clear reflections in Figure 3a and the relatively sharp peaks in the semblance plot of Figure 3b, resolution of stacking velocities was quite good for events above 250 ms two-way traveltime, while velocity resolution was poor for greater traveltimes. The stacking velocity field (Figure 4b) used to NMO correct P-wave data shows lateral and vertical changes, ranging from 1850 to 2450 m/s. The most prominent are the vertical changes, which occur at the interfaces, while lateral changes are confined almost exclusively in the near surface. The lack of resolution in the velocity analysis, due to the too short maximum offset we used to collect the data, introduced inevitable uncertainties in velocity values, preventing a well-defined seismic imaging at depths greater than 250 ms two-way traveltime. Prestack processing was completed with the application of residual static corrections. Five iterations of surface-consistent statics with a maximum allowable static shift of ± 5 ms improved the continuity of the seismic horizons.

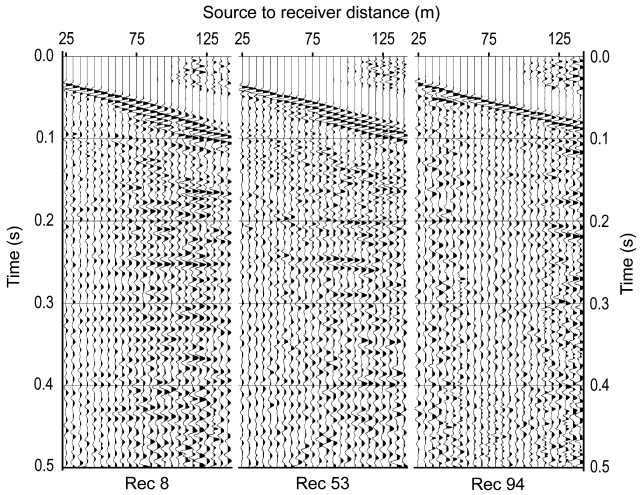

Figure 2. The same records as Figure 1, after Butterworth filtering and *f–k* muting to help remove the ground roll.

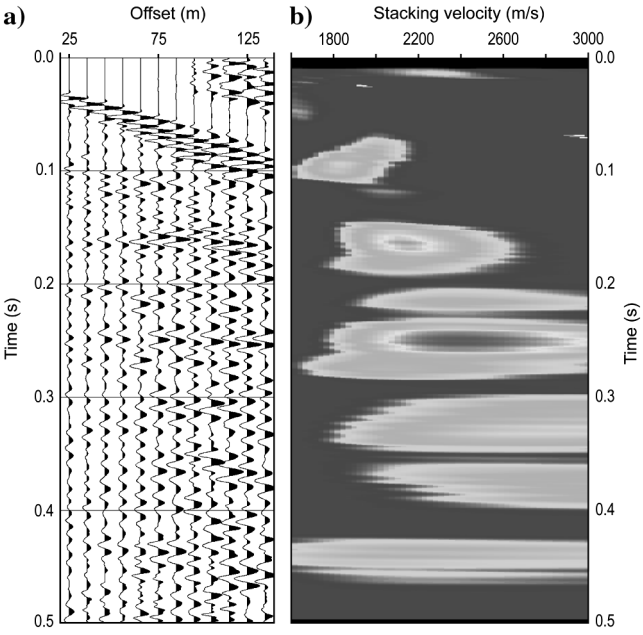

Figure 3. (a) CMP gather 54 with (b) its velocity spectrum (semblance plot).

The CMP stacked time section obtained with this data set reveals a simple stratigraphic framework along the survey line (Figure 4a). Several reflections are visible throughout the entire section, although not always continuous; in the near-surface, down to about 140 ms two-way traveltime, they appear as flat events, while at greater depths the more continuous reflections are dipping events. The shallowest reflection, with onset of about 60 ms two-way traveltime, is continuous from the beginning of the section up to the distance of 350 m, where it disappears or its amplitudes become too low. The second flat reflection (onset of 120 ms) is evident only beyond the progressive of 200 m. Below it, in a system of dipping reflectors being more or less continuous, the one with the highest amplitudes starts at the beginning of the section with onset of about 250 ms and shallows up to 190 ms at the end of the section. For this event, too, amplitudes greatly change along the section. Deeper reflectors are also evident, but they appear very discontinuous, probably because stacking velocities we used to NMO correct them were not good.

CRS processing

We produced the CRS stacked section in an entirely data-driven way starting with the same preprocessed data we used for the conventional CMP imaging. The only data we supplied were the dominant frequency of the reflected signals (70 Hz), the mean value of the near-surface velocity along the seismic line (1900 m/s), and, to minimize the computational effort, the range of the expected stacking velocities (1800–3000 m/s). In estimating the optimized CRS attributes (α, R_{NIP}, R_N) we paid great attention to the determination of the appropriate aperture values. Because no stretch effects were expected to be generated by the CRS stack, along the offset direction we used a fixed aperture of 140 m for all traveltimes coinciding with the maximum available offset for our data. Along the midpoint direction, we used a time-dependent aperture increasing with depth. We initially started using a test aperture range between 26 m ($t = 0$) and 100 m ($t = t_{\max}$). Afterward, we analyzed an output section that displays the ratio between our chosen aperture and the approximate size of the first Fresnel zones, which is calculated by the CRS-stack software for each output sample. The goal was to find an aperture not larger than the first Fresnel zone and as small as image quality and stacking parameter reliability would allow. In this way, by checking the quality of the results through the analysis of both the stacked and coherence (semblance) sections, we iteratively changed the midpoint aperture range to get optimum minimum and maximum apertures of 20 and 70 m, respectively. Finally, to remove fluctuations and outliers, we repeatedly updated CRS parameters by applying an event-consistent smoothing (Hertweck et al., 2005) and running the stacking parameter optimization code. To enhance the coherency of the reflected signals on the stacked section refining the kinematic wavefield attributes, we applied a CRS-stack-based residual static correction (Koglin et al., 2006) within the

CRS-stack workflow, and using the same threshold adopted in the standard CMP processing (with a maximum allowable static shift of ±5 ms). The event-consistent smoothing method used in updating CRS parameters also helped to avoid unreliable time shifts. The result of the whole procedure is the CRS-stacked section shown in Figure 5. In this section, all reflectors already highlighted in Figure 4, but also at greater depths, are imaged well. Moreover, all of them, from the shallowest down to the deepest one, have a greater continuity and an increased S/N compared to the ones imaged in the CMP section. The CRS stacked section appears more suitable to delineate the aquifer and its confining units in this case history.

Although the CRS stack is able to produce stacked sections without any preliminary explicit velocity analysis, interval velocities are usually requested to characterize and interpret the subsurface. Therefore, we also estimated the velocity field using kinematic information put out by the CRS stack. Our aim was to make a more exhaustive comparison between the two procedures used in this work. For this purpose, we used the tomographic inversion method as proposed by Duveneck (2004). Starting from the CRS parameters picked at several locations in the stacked (zero-offset) section, we determined the macrovelocity model (Figure 6a) using a least-squares minimization of the misfit between the picked and forward-modeled attributes. In comparison with the interval velocity field (Figure 6b) obtained applying the Dix equations (Dix, 1955) to the stacking velocity field computed by the standard CMP velocity analysis, velocities change in a wider range that reaches higher values in the deepest portion of the section. Moreover, the CRS-derived velocity field is more laterally structured than the standard one.

FIELD EXAMPLE 2: ULTRASHALLOW SH-WAVE DATA SET

Standard CMP processing

The data set described here was collected in a high-resolution SH-wave reflection survey to delineate the overburden-bedrock surface as well as reflectors within the overburden. It also gives accurate shear-wave velocities needed to estimate geotechnical properties of the overburden materials. The data were recorded with a 24-channel seismograph using 100 Hz natural-frequency special horizontal detectors (Sambuelli et al., 2001). The source was a 70-kg steel plate with ground grippers, struck at only one side (along a direction perpendicular to the seismic line) by an 8 kg sledgehammer. An off-end spread with a group interval of 0.5 m was used, with offsets ranging from 1 to 12.5 m. Three representative shot gathers are shown in Figure 7.

Reflections are evident above 200 ms. In the shot gathers of the first part of the line, up to record 20, five reflections (events *a*, *b*, *c*, *d*, and *e*) are evident while in the others only three events (*a*, *b*, and *e*) are present. The data were generally of high quality, so they required relatively simple preprocessing. This included assignment of field geometry, trace editing, first-arrival mute, and Butterworth filtering (60–200 Hz, 24 dB/octave), mainly aimed at attenuating Love waves and high-frequency noises. Like in the previous case, neither elevation nor refraction statics were applied at this stage because of the flat site topography. We considered them as residual statics because they have wavelengths shorter than the spread length.

The main processing flow consisted of velocity analysis, NMO corrections, NMO-stretch muting, residual statics, and CMP

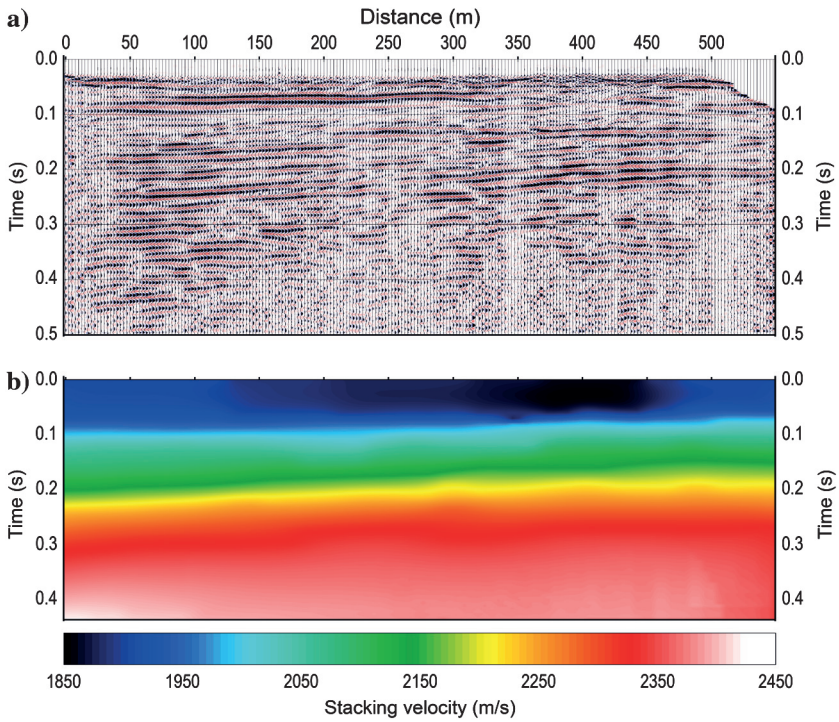

Figure 4. (a) CMP stacked time section. (b) Stacking velocity field obtained through integrated analysis of constant velocity scan, constant velocity stacks, and semblance plots. The velocity map, defined for all time samples up to 400 ms two-way traveltime and all CMPs, was generated by interpolation of the time-velocity curves spaced along the seismic line.

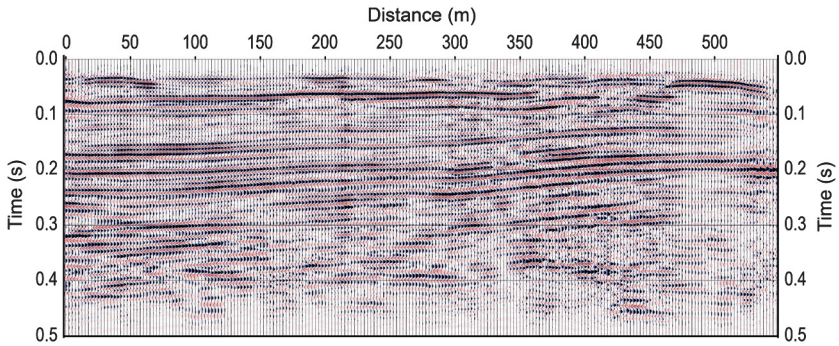

Figure 5. CRS-stacked section.

stacking; no poststack processing was applied. As it often occurs, the detailed velocity analysis proved to be the most important and time-consuming processing step in the conventional CMP stacking procedure. The initial velocity models were developed through integrated analysis of constant velocity gathers, constant velocity stacks, and semblance plots. In doing this, stacking velocities ranged from 70 to 140 m/s with an increment of 1 m/s. A variation of only 2–4 m / s in stacking velocity, easily seen in NMO-corrected CMP gathers (Figure 8), can significantly distort the stack results.

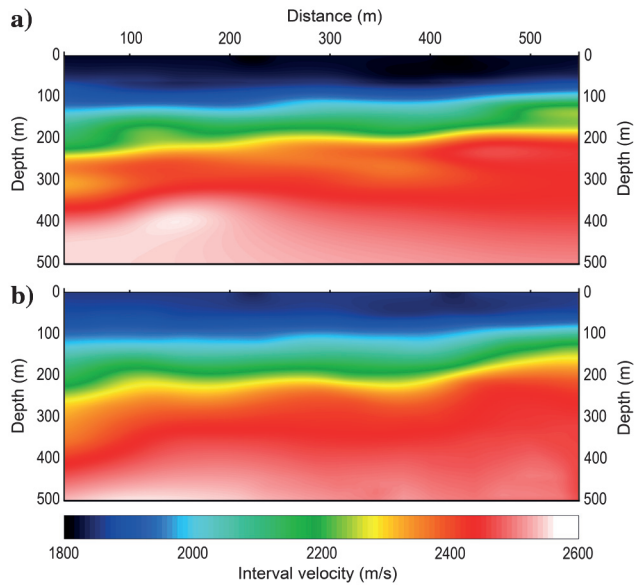

Figure 6. (a) Smooth macrovelocity model obtained by tomographic inversion. (b) Interval velocities derived from the stacking velocity field in Figure 4b using the Dix equations.

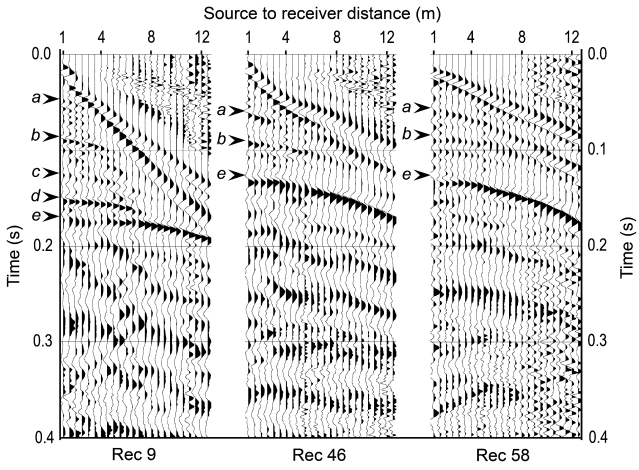

Figure 7. Raw shot gathers from three locations along the line. For display purposes, AGC scaling with a 60 ms window has been applied. The events marked *a*, *b*, *c*, and *d* are the reflections from interfaces inside the overburden material; event *e* is the bedrock reflection. Reflection *a* is visible at the very near offsets or appears very close to the direct or refracted waves. Notice that first arrivals show evidence of strong near-surface velocity changes.

Hand-picked first arrivals supplied additional information on near-surface velocities. To minimize the detrimental effects of the stretching process, e.g., reduction of the dominant frequency bandwidth and distortion of the amplitude of the reflection wavelet, the NMO corrections were performed with a stretch mute, limiting the allowable stretch to 25%. Moreover, to improve the coherency of the stacked data, a surface-consistent statics routine with a 2 ms (equivalent to about 1/5 of the dominant period) maximum allowable static shift was used.

The reflections observed on the shot gathers in Figure 7 are imaged well on the stacked time section shown in Figure 9. Above the strongest and deepest reflector (the bedrock surface — event *e*), which dips from 127 ms at the eastern end of the section to 170 ms at the western end, other flat-lying events are imaged at 150 ms (event *d*), 125 ms (event *c*) and 88 ms (event *b*). Event *a*, at 50 ms two-way traveltime, however, is not imaged well, probably because very few traces per record contain this signal, or because it was partially muted performing the first-arrival (due to their closeness) and/or the stretch muting.

Optimum stacking velocities along the line are displayed in Figure 9b. Vertical and lateral changes in velocity are evident from the ground surface down to the deepest reflector, ranging from 88 to 130 m/s. The very low SH-wave velocities and the high quality of reflection data allowed the detailed imaging of the subsurface at this site.

CRS processing

We input the same preprocessed data as for the standard CMP procedure. For the CRS processing, conventional velocity analysis and NMO-stretch muting were not required. The mean value (90 m/s) of near-surface velocities above the shallower reflector and the dominant frequency (80 Hz) of the reflected signals were the only information we supplied. Several tests were made to evaluate the optimum CRS apertures along offset and midpoint axes. Finally, we chose to use for all traveltimes the maximum available offset of 12.5 m, and a midpoint aperture that increased with time from 1 to 5 m. We checked that these values were always smaller

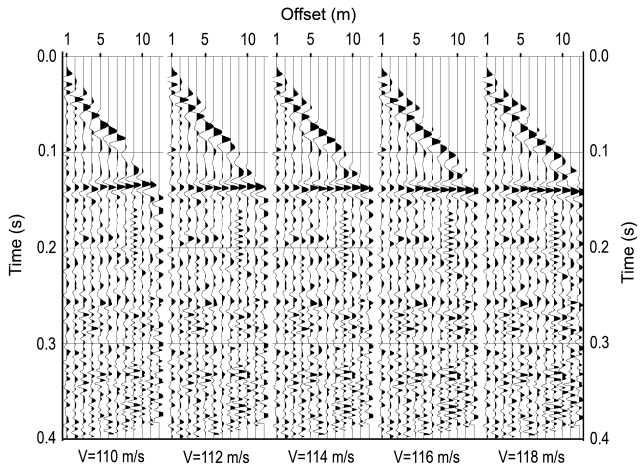

Figure 8. Constant velocity scan (velocity analysis) of CMP gather 92; it has been dynamically corrected using five different velocities to show the precision necessary during the velocity analysis stage of the processing flow. Stacking velocity of 114 m/s appears the best stacking velocity for the bedrock reflection.

than the predicted size of the first Fresnel zone. We completed the CRS processing with a CRS-stack-based surface-consistent statics routine, one with the same maximum allowable static shift (±2 ms) we used in the standard CMP processing. The resulting stacked section is displayed in Figure 10.

The reflections pointed out in Figure 7 are imaged well in this case too. All events appear coherent and continuous; in particular, the shallowest reflection (event *a*) has a greater continuity here than the one shown in the CMP stacked section. The CRS stacked section, however, appears more smoothed (lateral smearing) than the standard CMP section, probably because of the use of supergathers. In some portions of the section, this lateral smearing seems to lower the resolution. That is, the CRS stack seems to act as a spatial high-cut filter, so that the stacked traces look like the ones obtainable with a poststack mixing-trace processing step. Events *c* and *d*, for example, are unresolved, and the pinchout at the distance of about 11 m along the line is not imaged so well as in the CMP-stacked section (Figure 9a). Moreover, it also produces some alignments below the top of the bedrock, probably due to poorly attenuated surface multiples.

In this case, to retrieve the velocity field we picked the two-way traveltime of reflected events directly on the CRS stacked section because this guaranteed the use of only the optimized and smoothed CRS parameters related to the actual reflected events. The high S/N of the CRS stacked section helped us to better identify actual reflections, and the coherence section allowed a quick identification and removal of outliers. The estimated CRS velocity field (Figure 10b) appears more smoothed but very similar to the one shown in Figure 9b, which shows approximately the same range of values, from 88 to 120 m/s.

DISCUSSION

The CRS stack has the advantage of using more traces than the conventional CMP processing to produce a stacked section. In fact, it has a multiple-CMP fold along the midpoint direction as it stacks traces from multiple CMP gathers, and it preserves higher-CMP fold along the offset direction because the CRS stack avoids the detrimental effects of the stretching process on shallow reflections at larger offsets (Mann and Höcht, 2003). In this way, it can achieve better S/N than could a CMP stack. In high-resolution shallow seismic reflection surveys, however, this advantage could partially turn into a drawback. Near-surface materials often exhibit large horizontal and vertical velocity gradients as well as strong anelastic attenuation. As source-to-receiver

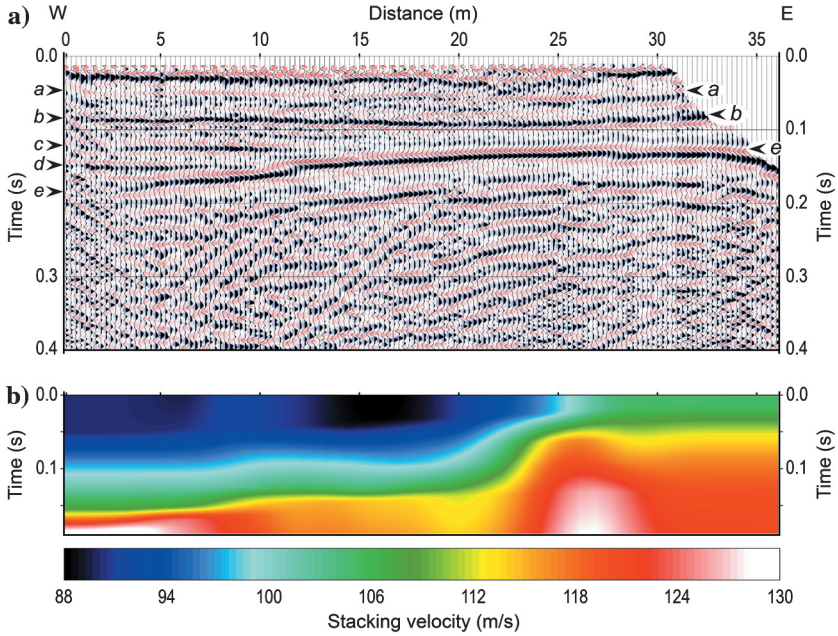

Figure 9. (a) CMP-stacked time section. All reflections appear resolved well throughout the section, and two of them show a very well-defined pinch-out with the bedrock. The shallowest reflection, however, is less clear: only the troughs (red) of the wavelet are clearly visible. (b) Velocity field used to apply the moveout correction to the time section.

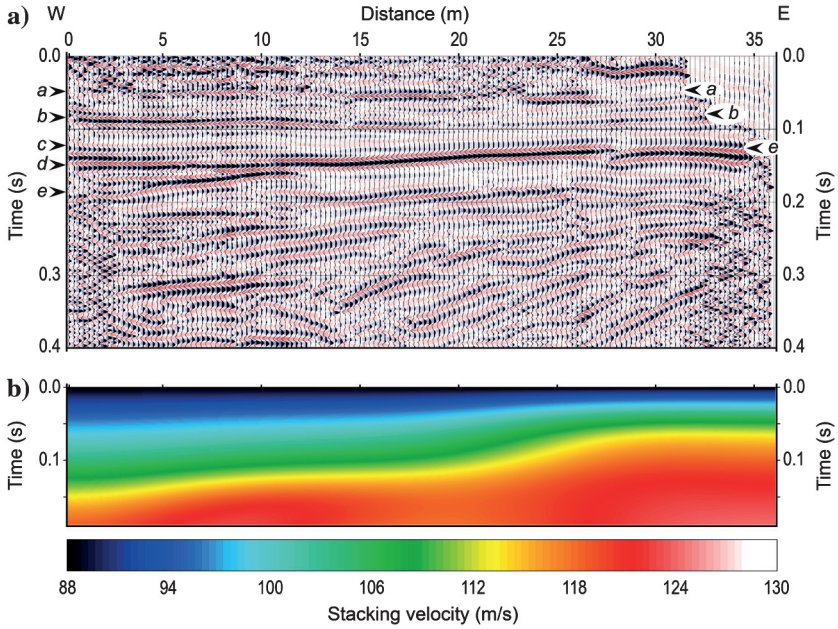

Figure 10. (a) Final CRS stacked time section obtained after two optimization steps. Reflections *c* and *d* appear unresolved and the pinchouts are not imaged well. The bedrock reflection (event *e*) also shows a discontinuity at the distance of about 27 m, probably due to unresolved static errors. The shallowest reflection, however, is here more evident than in Figure 9a. (b) Final velocity field obtained from the CRS attributes after regularization. The color velocity scale is the same used for Figure 9b, to allow an easier comparison between the velocity fields.

offset increases, reflected traveltimes may be distorted by residual statics that may be partially nonsurface-consistent, while amplitude and phase of shallow and ultrashallow reflected signals may rapidly change. Moreover, since reflections from shallow and ultrashallow interfaces are often supercritical reflections, reflection coefficients become complex and induce other phase changes in reflected signals, making the solution of residual statics more complicated and not completely achievable. Therefore, summing many traces, reflected signals can undergo a high-cut filtering, which necessarily brings down seismic resolution, negatively affecting CRS parameters and, as a consequence, the velocity field as well. Smaller apertures should reduce this drawback but, unfortunately, they lower the S/N. A careful preliminary analysis of shot gathers should be very helpful to choose apertures for the best trade-off between seismic resolution and S/N, specifically when subsurface discontinuities have to be preserved.

The CRS stack does not require manual picking in velocity spectra or a priori information concerning the unknown macrovelocity model to produce stacked sections. Consequently, in comparison with the conventional CMP stack, it can be implemented faster and in a less user-interactive way. It achieves a high degree of automatization and lowers costs for data processing. Nowadays, moreover, the high degree of automatization makes the CRS method very suited for real time processing (Heilmann et al., 2009). The possibility of processing data in real time in the field is particularly important in shallow surveys because efficient data acquisition can require dynamic adjustments. This is such an important objective that geophysicists as far back as 15 years ago already hoped for it (Steeples et al., 1997).

CONCLUSIONS

The objective of this contribution was to investigate the possibility of obtaining a detailed image of shallow and ultrashallow subsurface structures using the data-driven CRS stack. Case histories we describe for P- and SH-waves show that our method allows for obtaining high-quality stacked sections suitable for a subsurface interpretation, at least for a preliminary interpretation. The greater cost efficiency of the CRS stack makes it a valuable alternative to the CMP stack, even if at the cost of losing a little resolution when, for example, residual statics cannot be completely resolved. Velocity fields have been reconstructed in detail as well, even though with more time (specifically for the P-wave case, for which we used the tomographic approach) than that required to produce the stacked sections. Therefore, we can certainly affirm that the CRS stack, combined with one of the high production rate data acquisition systems now available, would make the shallow seismic reflection method an economical option, having a wide appeal for engineers, geotechnicians, and hydrogeologists.

ACKNOWLEDGMENTS

We are very grateful to Jürgen Mann for providing the 2D CRS code and his useful comments, and to Tilman Klüver for making the NIP tomography code available. These codes were used with Seismic Unix, Center for Wave Phenomena, Colorado School of Mines. Our thanks go to Manuela Mendes who kindly reviewed the draft of this manuscript and gave us valuable and helpful suggestions. The authors also thank Claudio Strobbia, Stefan Carpentier, and two anonymous reviewers for their critical, accurate, and very constructive remarks, which helped to improve the manuscript in many details. This work was partially carried out in the framework of GRIDA3 research project.

REFERENCES

Baykulov, M., S. Dümmong, and D. Gajewski, 2011, From time to depth with CRS attributes: Geophysics, **76**, no. 4, S151–S155, doi: 10.1190/1.3580607.

Benjumea, B., J. A. Hunter, J. M. Aylsworth, and S. E. Pullan, 2003, Application of high-resolution seismic techniques in the evaluation of earthquake site response, Ottawa Valley, Canada: Tectonophysics, **368**, 193–209, doi: 10.1016/S0040-1951(03)00158-6.

Bergler, S., 2004, On the determination and use of kinematic wavefield attributes for 3D seismic imaging: Logos Verlag.

Bergler, S., P. Hubral, P. Marchetti, A. Cristini, and G. Cardone, 2002, 3D common-reflection-surface stack and kinematic wavefield attributes: The Leading Edge, **21**, 1010–1015, doi: 10.1190/1.1518438.

Bradford, J. H., L. M. Liberty, M. W. Lyle, W. P. Clement, and S. Hess, 2006, Imaging complex structure in shallow seismic-reflection data using prestack depth migration: Geophysics, **71**, no. 6, B175–B181, doi: 10.1190/1.2335659.

Bradford, J. H., and D. S. Sawyer, 2002, Depth characterization of shallow aquifers with seismic reflection, Part II — Prestack depth migration and field examples: Geophysics, **67**, 98–109, doi: 10.1190/1.1451372.

Bruno, P. P., A. Castiello, and L. Improta, 2010, Ultrashallow seismic imaging of the causative fault of the 1980, M6.9, southern Italy earthquake by pre-stack depth migration of dense wide-aperture data: Geophysical Research Letters, **37**, L19302, doi: 10.1029/2010GL044721.

Dix, C. H., 1955, Seismic velocities from surface measurements: Geophysics, **20**, 68–86, doi: 10.1190/1.1438126.

Duveneck, E., 2004, Velocity model estimation with data-derived wavefront attributes: Geophysics, **69**, 265–274, doi: 10.1190/1.1649394.

Gelchinsky, B., A. Berkovitch, and S. Keydar, 1999a, Multifocusing homeomorphic imaging — Part 1. Basic concepts and formulas: Journal of Applied Geophysics, **42**, 229–242, doi: 10.1016/S0926-9851(99)00038-5.

Gelchinsky, B., A. Berkovitch, and S. Keydar, 1999b, Multifocusing homeomorphic imaging — Part 2. Multifold data set and multifocusing: Journal of Applied Geophysics, **42**, 243–260, doi: 10.1016/S0926-9851(99)00039-7.

Ghose, R., V. Nijhof, J. Brouwer, Y. Matsubara, Y. Kaida, and T. Takahashi, 1998, Shallow to very-shallow, high-resolution reflection seismic using a portable vibrator system: Geophysics, **63**, 1295–1309, doi: 10.1190/1.1444431.

Gierse, G., H. Trappe, J. Pruessmann, and G. Eisenberg-Klein, 2009, Enhanced velocity analysis, binning, gap infill, and imaging of sparse 2D/3D seismic data by CRS techniques: 79th Annual International Meeting, SEG, Expanded Abstracts, 3279–3283.

Goforth, T., and C. Hayward, 1992, Seismic reflection investigations of a bedrock surface buried under alluvium: Geophysics, **57**, 1217–1227, doi: 10.1190/1.1443337.

Guy, E. D., R. C. Nolen-Hoeksema, J. J. Daniels, and T. Lefchik, 2003, High-resolution SH-wave seismic reflection investigations near a coal mine-related roadway collapse feature: Journal of Applied Geophysics, **54**, 51–70, doi: 10.1016/S0926-9851(03)00055-7.

Heilmann, B. Z., A. M. Vallenilla Ferrara, G. Satta, and E. Bonomi, 2009, Eiagrid: In-field optimization of seismic data acquisition by real-time subsurface imaging using a remote grid computing environment: 11th International Congress of the Brazilian Geophysical Society, Extended Abstracts.

Heilmann, Z., J. Mann, and I. Koglin, 2006, CRS-stack-based seismic imaging considering top-surface topography: Geophysical Prospecting, **54**, 681–695, doi: 10.1111/gpr.2006.54.issue-6.

Hertweck, T., J. Mann, and T. Klüver, 2005, Event-consistent smoothing in the context of the CRS stack method: Journal of Seismic Exploration, **14**, 197–215.

Hertweck, T., J. Schleicher, and J. Mann, 2007, Data stacking beyond CMP: The Leading Edge, **26**, 818–827, doi: 10.1190/1.2756859.

Höcht, G., 2002, Traveltime approximations for 2D and 3D media and kinematic wavefield attributes: Ph.D. thesis, University of Karlsruhe.

Hubral, P., 1983, Computing true amplitude reflections in a laterally inhomogeneous earth: Geophysics, **48**, 1051–1062, doi: 10.1190/1.1441528.

Jäger, R., J. Mann, G. Höcht, and P. Hubral, 2001, Common-reflection-surface stack: Images and attributes: Geophysics, **66**, 97–109, doi: 10.1190/1.1444927.

Koglin, I., J. Mann, and Z. Heilmann, 2006, CRS-stack-based residual static correction: Geophysical Prospecting, **54**, 697–707, doi: 10.1111/gpr.2006.54.issue-6.

Liberty, L., 1998, Seismic reflection imaging of a geothermal aquifer in an urban setting: Geophysics, **63**, 1285–1294, doi: 10.1190/1.1444430.

Mann, J., 2002, Extensions and applications of the common-reflection-surface stack method: Ph.D. thesis, University of Karlsruhe.
Mann, J., and G. Höcht, 2003, Pulse stretch effects in the context of data-driven imaging methods: 65th Exhibition and Conference, EAGE, Session P007.
Mann, J., R. Jäger, T. Müller, G. Höcht, and P. Hubral, 1999, Common-reflection-surface stack — a real data example: Journal of applied geophysics, **42**, 301–318, doi: 10.1016/S0926-9851(99)00042-7.
Pasasa, L., F. Wenzel, and P. Zhao, 1998, Prestack Kirchhoff depth migration of shallow seismic data: Geophysics, **63**, 1241–1247, doi: 10.1190/1.1444425.
Perroud, H., and M. Tygel, 2005, Velocity estimation by the common-reflection-surface (CRS) method: Using ground-penetrating radar data: Geophysics, **70**, no. 6, B43–B52, doi: 10.1190/1.2106047.
Pruessmann, J., S. Frehers, R. Ballesteros, A. Caballero, and G. Clemente, 2008, CRS-based depth model building and imaging of 3D seismic data from the Gulf of Mexico Coast: Geophysics, **73**, no. 5, VE303–VE311, doi: 10.1190/1.2968691.
Pugin, A. J. -M., S. E. Pullan, J. A. Hunter, and G. A. Oldenborger, 2009, Hydrogeological prospecting using P- and S-wave landstreamer seismic reflection methods: Near Surface Geophysics, **7**, 315–327.
Sambuelli, L., G. P. Deidda, G. Albis, E. Giorcelli, and G. Tristano, 2001, Comparison of standard horizontal geophones and newly designed horizontal detectors: Geophysics, **66**, 1827–1837, doi: 10.1190/1.1487125.
Steeples, D. W., A. G. Green, T. V. McEvilly, R. D. Miller, W. E. Doll, and J. W. Rector, 1997, A workshop examination of shallow seismic reflection surveying: The Leading Edge, **16**, 1641–1647, doi: 10.1190/1.1437543.
van der Veen, M., and A. G. Green, 1998, Land streamer for shallow seismic data acquisition: Evaluation of gimbal mounted geophones: Geophysics, **63**, 1408–1413, doi: 10.1190/1.1444442.
van der Veen, M., R. Spitzer, A. G. Green, and P. Wild, 2001, Design and application of a towed landstreamer for cost-effective 2D and pseudo-3D shallow seismic data acquisition: Geophysics, **66**, 482–500, doi: 10.1190/1.1444939.
Woorely, E. W., R. L. Street, Z. Wang, and J. B. Harris, 1993, Near-surface deformation in the New Madrid seismic zone as imaged by high resolution SH-wave seismic methods: Geophysical Research Letters, **20**, 1615–1618, doi: 10.1029/93GL01658.
Zhang, Y., S. Bergler, and P. Hubral, 2001, Common-reflection-surface (CRS) stack for common-offset: Geophysical Prospecting, **49**, 709–718, doi: 10.1046/j.1365-2478.2001.00292.x.